ISSN: 0067-2904

Synthesis, Characterization and Evaluation the Biological Activities of some new Transition Metal Complexes with Organic Ligand formamidine

Ghadeer Alataby*, Areej Kamal Assim Aldabbagh
Department of Chemistry/ College of Science for Woman, University of Baghdad, Baghdad, Iraq.

Received: 9/3/2024 Accepted:16/1/2025 Published: 30/1/2026

Abstract

Novel formamidine transition metal complexes were synthesized and thoroughly investigated through a reaction between various metal ions (Mn(II), Fe(II), Pd(II), Rh(III), Pt(IV), and Mo(VI)) and N,N-bis-(m-nitroaniline), resulting in air-stable complexes with geometrically distinct structures, including octahedral arrangements for Fe(II), Rh(III), Pt(III), and Mo(VI), a square planar configuration for Pd(II), and a tetrahedral structure for Mn(II). The structures of these compounds were identified using various techniques. IR spectra verified how the formamidine group act as bidentate N_2 ligand chelating with the metal ions. Mass spectroscopy confirmed the suggested geometries. Studies have done by pyrolysis (TGA and DSC curve) shown that water excesses could be coordinated with metal complexes. ^{1}H-NMR and magnetic sensitivity have also confirmed the existence of the ligand (HL) and consequently complexation with the metals. Besides, elemental micro-analysis, ultraviolet-visible spectroscopy, conductivity and melting points examination were implemented. The antioxidant activity of the compounds was finally assessed using the DPPH as free radical method. Gallic acid was used as a standard substance, has determined an IC_{50} value for the achieved complexes, which are potentially able to DPPH scavenge free radicals. Biological activity of the prepared ligand and its synthesized complexes has assessed against bacterial species, one of Gram-positive bacteria and the other was Gram negative bacteria, as well as fungi screening. The ligand [LNO2] did not appear to exert any effort towards the Stab positive bacteria and the Esch negative bacteria at the concentration used, while the participation of the complexes was higher compared to the ligand next to the positive and negative bacteria in concentration. The hostility of iron, rhodium and molybdenum was not observed at the concentration of the complexes and even the participation of platinum in the bacteria. Only the gram negative was not given to the body, knowing that the metal salts were more effective than the ligand. Inhibition of the ligand [HLNO2] against the fungus.

Keywords: Antioxidant measurements, antibacterial and anti-fungi evaluation, formamidine ligands, mass spectroscopy, main transition complexes.

تحضير وتشخيص وتقييم الفعاليه البايولوجية لمعقدات جديدة لبعض العناصر الانتقالية مع ليكاند عضوي جديد

غدير العتابي* ، اريج كمال
قسم الكيمياء ,كلية العلوم للبنات , جامعة بغداد

*Email: alatabyghadeer@gmail.com

الخلاصة

تم تخليق وتوصيف سلسلة جديدة من معقدات المعادن الانتقالية للفورماميدين (N,N–bis–(*m*–nitroaniline. التفاعل بين مركب الفورماميدين والأيونات المعدنية التالية: (المنغنيز (II)، الحديد (II)، البلاديوم (II)، الروديوم (III)، البلاتينيوم (IV) والمولبيديوم (VI)) أدى إلى تخليق معقدات مستقرة تجاه الهواء ذات شكل ثماني السطوح (الحديد (II)، الروديوم (III)، البلاتينيوم (IV) والمولبيديوم (VI)) والشكل المربع المستوي للبلاديوم (II)، والشكل رباعي السطوح للمنغنيز (II). تم التعرف على اشكال هذه المركبات باستخدام تقنيات مختلفة. أظهرالتحليل الطيفي باستخدام الأشعة تحت الحمراء كيفية تشكل ليكاند الفورماميدين كمركب ثنائي السن N_2 وكيفية تناسقها مع الأيونات المعدنية. تم تشخيص هذه المركبات باستخدام التحليل الطيفي الوزني، والذي أثبت صحة الشكل الهندسي المقترح. أثبتت الدراسات التي تستخدم الانحلال الحراري (DSCوTGA) أن بقايا الماء يمكن ان تتناسق مع المعقدات المعدنية. كشف فحص المركبات باستخدام تقنيه الرنين النووي المغناطيسي البروتوني والحساسية المغناطيسية أيضًا عن وجود التناسق مع المعادن وتكوين المركب (HL). بالإضافة إلى ذلك، استخدم التحليل الدقيق للعناصر، التحليل الطيفي للأشعة فوق البنفسجية والمرئية، الموصلية وفحص درجات الانصهار. تم تقييم خصائص المركبات كمضادات للأكسدة باستخدام DPPH كطريقة جذور حرة. وقد تم استخدام حمض الكاليك كمادة قياسية، حيث حددت قيمة IC_{50} للمجمعات المحققة. هذه المعقدات لديها القدرة على DPPH كسح الجذور الحرة. تم أخيرًا فحص الليكاند المحضر ومعقداته المعدنية من حيث نشاطها البيولوجي ضد أنواع بكتيرية إحداها بكتريا موجبة الجرام والأخرى سالبة الجرام وكذلك الفطريات. الليكاند [L^{NO2}] لم يظهر أي تثبيطاً تجاه البكتريا الموجبة Stap والبكتريا السالبة Esch عند التركيز المستخدم، في حين أظهرت المعقدات تثبيط أعلى مقارنة بالليكاند تجاه البكتريا الموجبة والسالبة في التركيز عدا معقد الحديد والروديوم والموليبدنوم لم يظهر تثبيط عند التركيز للمعقدات وايضا معقد البلاتين في بكتريا سالبة الكرام فقط لم يُعط تثبيطاً، علما ان الاملاح الفلزات كانت فعاليتها أعلى من الليكاند. يظهر تثبيط لليكاند [HL^{NO2}] تجاه الفطر.

1. Introduction:

In 1858, Gerhardt prepared amidines ($R^2N=C(R^1)–NHR^3$) firstly the aniline and N-phenylbenzimidyl chloride reaction [1]. Amidines are important organic compounds utilized in synthetic chemistry as basic intermediates and starting materials [2]. Specifically, when R1= H in an amidine, the ligand is classified as formamidine [3]. These ligands are particularly valuable due to their ease of crystallized, diverse coordination modes, and can be produced in large quantities [4]. Formamidines in particular are chemicals widely used in the pharmaceutical and medical fields [5]. Specifically, amidine (N-H deprotonated amidines) products have shown promise as chemical vapor deposition (Chemical vapor deposition) precursors [6]. Over the past decade, N, N'-chelating organic ligands have gained more and more attention in the field of organometallic chemistry because of their versatility in coordinating a wide range of main-group f-block and transition metal centers [7]. Their prevalence is attributed to the ease with which their steric and electrical properties can be adjusted by changing the organic substituents R and R'[8]. Additionally, amidines possess a strong ability to form complexes with metals, in addition to their supporting roles in asymmetric synthesis [9 and 10]. Despite the possible issues brought on by their high basicity, a variety of tiny amidine compounds with basic functional groups have been identified for over a decade as efficient nucleophilic catalysts in organic synthesis [11 ,12].

In this work we report the synthesis, characterization, spectroscopic analysis, thermal decomposition (TGA and DSC curve), and the antioxidant activity of formamidine metal complexes with (Mn (II), Fe (II), Pd (II), Rh (III), Pt (IV) and Mo (VI)). The antioxidant activity was evaluated against the DPPH compared to that of a reference natural antioxidant gallic acid. Additionally, the biological activity of the formamidine complexes examine two

kinds of bacteria *Escherichia coli* as Gramme negative bacteria, and *Staphylococcus aurous* as Gramme positive bacteria, as well as fungi test.

2.Experimental

2.1Materials and Methods:

The trading suppliers, Sigma, Aldrich, and Merck, provided the materials. 1 x 10^{-3} M. DMSO, THF, and DMF were the solvents, have all been used. The ^{1}H-NMR spectra were obtained using the Bruker (400 MHz) Spectrometer. Fourier transform was examined using the IR Prestige-21. The UV-1800 Shimadzu Spectrophotometer was used to acquire the UV-visible absorption spectra. All of the products' mass spectra have been gathered using (MS) Q-P-50-A-D-I Analysis. Mass spectrometer Shimadzu QP (E170Ev) -2010-Pluss. Metals were identified using a Shimadzu (A.A) 680 G atomic clock. The complementary susceptibility model MSR-MKI was engaged to detect the magnetic properties for the complexes. For the thermal analysis of all earlier types, Perkin-Elmer Pyres Diamond TGA-DSC was utilized. To perform (C.H.N) analysis, the Revector model EA/3000, singleV3O, was utilized. Melting points were performed to know the stability of the final products and were incorrect. The conduct meter W-T-W, 25°C has been used to quantify molar conductivity.

2.2Synthesis of N, N-bis-(m-nitroaniline)-formamidine Ligand

This ligand was synthesized following a method from 1858,[13] with some amendments. The reaction performed by condensing (0.001mol/50g) of triethylorthoformate with (2 g, 0.002mol) of *m*-nitroaniline and adding about 10 drops of glacial acetic acid. The mixture kept stirring with reflex at a temperature of (60-70) °C for 4 hours. After half an hour of the reaction, the color changed to light brown. The precipitate was then filtered, collected, dried and recrystallized with ethanol offering the formamidine compound with light brown color, 85% yield and a melting point (190-192) °C.

2.3General Methodology for Metal Complexes Synthesis

To the prepared ligand, 1 g of NaOH was added and stirred at a low temperature without reflex for two hours, and upon completion, the precipitate was filtered. Metal salts (1 mmol) ($MnCl_2.4H_2O$ 0.1384 g, $FeSO_4.6H_2O$ 0.1872g) were dissolved in 10ml of water, ($(NH_4)_2MoO_4$ 0.1272g, $RhCl_3$ 0.1462g, $PdCl_2$ 0.240g, $H_2PtCl_6.6H_2O$ 0.1807g) were dissolved in 20ml of ethanol and 2 drop HCl, and added to the solution of the prepared formamidinate compound (NaL), which was dissolved in THF (0.423g, 2mmol) drop wise. The resultant mixture was allowed to cool and left stirring continuously for 3-4 days at room temperature. After isolating the solid precipitate from any unreacted components, gathered, dried and weighed. Schem.1 shows the formation steps starting from ligand preparing and ending with the metal complexes forming.

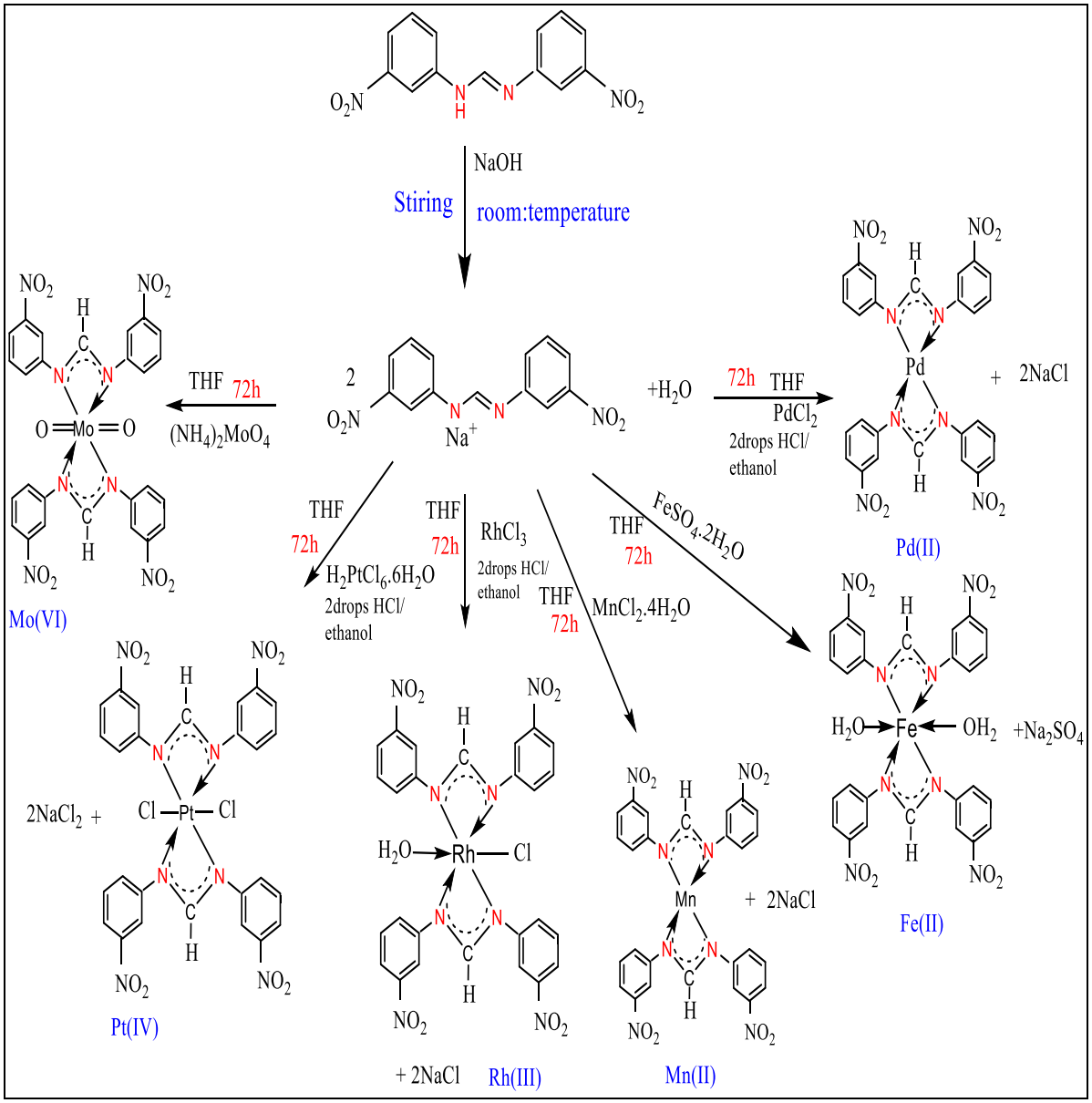

Scheme 1 : Synthesizing the ligand (HL) and their metal complexes.

3.Results and Discussion

Analytical and physical information regarding the synthesized complexes and the ligand (HL) was obtained from the ligand prepared from triethyl orthoformate and *m*-nitroaniline using 2 drops glacial acetic acid. Three types of reactions were performed using 1:1, 1:2, and 1:3, but the successful results were 1:2, and based on this, measurements of the preparation were made by diagnosis IR, UV, and mass spectrometry techniques. A number of solvents THF, DMSO, DMF when a solvent DMSO was used, it was difficult to evaporate were used, but the best result was THF Then reaction with metal salts by using THF solvent. Reaction of metal ions with ligand offered the synthesized complexes, shown in scheme.1 The outcomes of elemental analysis demonstrated that 1:2 M: L was the main quantity used for all produces, which agreed with the theoretical calculations, as shown in Table 1.

Table 1: Some elemental physical characteristics investigations of ligand and complexes

Complexes formula M. wt	C%	H%	N%	M%	Cl%	Conductivity In DMSO	Color	m.p °C
$C_{13}H_{10}N_4O_4$ 286.24	(54.55) 55.01	(3.52) 3.94	(19.57) 20.21				yellow	190-192
$C_{26}H_{18}N_8O_8Mn$ 625.41	(49.88) 50.18	(2.87) 2.18	(17.90) 17.08	(8.77) 7.99		18	Light brown	120-122 d
$C_{26}H_{22}N_8O_{10}Fe$ 662.35	(47.15) 48.09	(3.35) 4.11	(16.92) 17.82	(8.43) 7.93		13	Reddish brown	110-112 d
$C_{26}H_{20}ClN_8O_9Rh$ 726.84	(42.92) 43.08	(2.75) 3.45	(15.40) 14.97		(4.88) 5.44	10	Light brown	117-119 d
$C_{26}H_{18}N_8O_8Pd$ 676.89	(46.09) 45.66	(2.65) 3.77	(16.54) 17.59	(15.71) 14.77		18	Reddish brown	140-142 d
$C_{26}H_{18}Cl_2N_8O_8Pt$ 836.45	(37.3) 38.18	(2.15) 1.97	(13.38) 14.12	(23.31) 23.87	(8.48) 7.88	9	Dark brown	130-132 d
$C_{26}H_{18}N_8O_{10}Mo$ 698.41	(44.67) 45.28	(2.57) 2.08	(16.03) 15.88	(13.67) 14.27		15	Yellowish brown	135-137 d

Note* (Found)
d=decompose

3.1Proton Nuclear Magnetic Resonance Spectrum of the Ligand (^{1}H-NMR):

A spectrum ^{1}H-NMR of the ligand is shown in Fig. 1. The analysis was conducted using DMSO as a solvent, yielding a chemical shift of 2.48-2.49 ppm. Another shift appeared to be assigned to HDO(Hydrodeoxygenation) at 3.85 ppm. Multiple shifts appeared to be referred to the (C-H) aromatic between 7.20-8.60 ppm. It showed a peak in resonance (NH) 7.59 ppm(1H) [14 and 15].

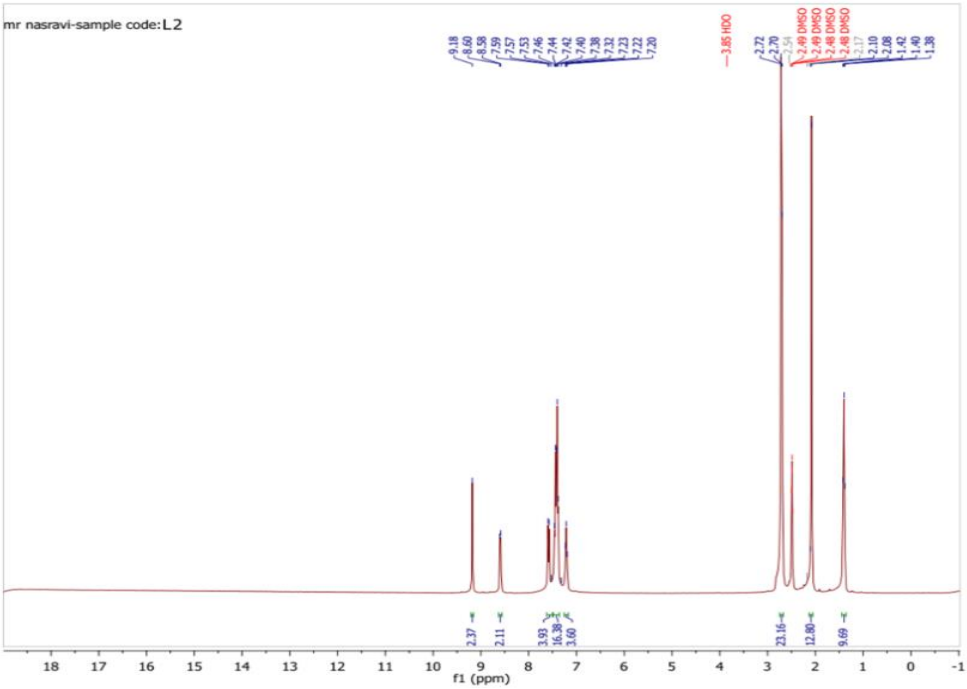

Figure 1 : ^{1}H-NMR spectra of ligand (HL)

3.2LC-Mass Spectrum of HL and Some of the complexes

LC-Mass measurements were employed to assess the ligand (HL) and some of the final products. This method was one of the most significant methods used for characterization and served as a complement to other methods that estimated the compound's molecular weight applying the relation (m/z). Scheme. 2. illustrates mass data for the ligand displaying the

extract mass and fragmentation pattern for each assembly. It can plainly detect the molecular ion peak $[M]^+$ for the portion $C_{13}H_{10}N_4O_4$ and its comparative copiousness about 15% in Fig. 2. Other peaks observed at 35%,30% belong to the $C_7H_4N_2O_2^{\bullet+}$, $C_6H_4N_2O_2^{\bullet+}$, respectively. For the $[Mn(L)_2]$ in Scheme. 3, It can be observed the molecular ion peak $[M^+]$ at 625.41 m/z with a comparative abundance of 10%, and the next patterns are $C_{26}H_{18}MnN_8O_8$, $C_{26}H_{17}MnN_7O_6$, $C_{20}H_{13}MnN_6O_4^+$, $C_7H_4MnN_2^+$, $C_7H_5N_2O_2^+$, $C_6H_5N_2O_2^+$, which correspond to 578.39 m/z,456.29 m/z,171.06 m/z, 149.13 m/z ,137.12 m/z, respectively. For the $[Fe(L)_2(H_2O)_2]$, Fig. 3 and Scheme. 4, we can observe the molecular ion peak $[M^+]$ at 662.35 m/z with a relative copiousness of 25%, and the next arrangements are $C_{26}H_{22}FeN_8O_{10}$, $C_{26}H_{17}FeN_8O_8^+$, $C_{26}H_{19}FeN_6O_4^+$, $C_{20}H_{15}FeN_5O_2^+$, $C_{14}H_{11}FeN_5O_2^+$, $CH_3FeN_3^+$, $C_7H_6N^+$, which correspond to 625.31 m/z ,535.31 m/z, 413.21 m/z ,337.11 m/z, 112.90 m/z ,104.13 m/z respectively [16]. For the $[(Pd(L)_2]$ in Fig.4 Scheme. 5 we can observe the molecular ion peak $[M^+]$ at 676.89 m/z with a relative abundance of 10%, and the next patterns are $C_{26}H_{18}N_8O_8Pd$, $C_{26}H_{18}N_6O_4Pd^{\bullet+}$, $C_{14}H_{10}N_4Pd^{\bullet+}$, $C_{13}H_{10}N_3Pd^{\bullet+}$, $C_7H_4N_2Pd^{\bullet+}$, which correspond to 584.88 m/z, 340.68 m/z, 314.66 m/z, 222.54 m/z respectively. For the $[Rh(L)_2(H_2O)(Cl)]$ Scheme. 6, we can observe the molecular ion peak $[M^+]$ at 726.84 m/z with a relative abundance of 10%, and the next patterns are $C_{26}H_{20}Cl_8O_9Rh$, $C_{26}H_{18}ClN_7O_6Rh^+$, $C_{20}H_{15}ClN_6O_4Rh^+$, $C_{20}H_{15}N_6O_4Rh^+$, $C_7H_4N_2Rh^+$, $C_7H_4N_2O_2^{\bullet+}$, $C_6H_5N_2O_2^+$, which correspond to 662.82 m/z ,541.73 m/z, 506.28 m/z ,219.03 m/z ,148.12 m/z ,137.12 m/z respectively [17]. For the $[Pt(L)_2(Cl)_2]$ Fig.5 Scheme. 7, we can observe the molecular ion peak $[M^+]$ at 836.45m/z with a relative abundance of 10%, and the next patterns are $C_{26}H_{18}Cl_2N_8O_8Pt$, $C_{26}H_{17}N_8O_8Pt^+$, $C_{26}H_{17}N_7O_6Pt^{\bullet+}$, $C_{20}H_{13}N_6O_4Pt^{\bullet+}$, $C_{13}H_8N_4O_4Pt^+$, which correspond to 764.54 m/z, 718.53 m/z, 596.43 m/z, 479.31 m/z respectively [18]. For the $[Mo(L)_2(O)_4]$ Scheme 8, we can observe the molecular ion peak $[M^+]$ at 698.41 m/z with a relative abundance of 20%, and the next forms are $C_{26}H_{18}MoN_8O_{10}$, $C_{26}H_{19}N_6O_6Mo^+$, $C_{26}H_{19}N_6O_5Mo^+$, $C_{20}H_{13}MoN_6O_5^+$, $C_6H_5N_2O_2^+$, $C_7H_6N^+$, which correspond to 607.41 m/z ,591.41 m/z ,513.29 m/z ,137.12 m/z, 104.13 m/z respectively [19].

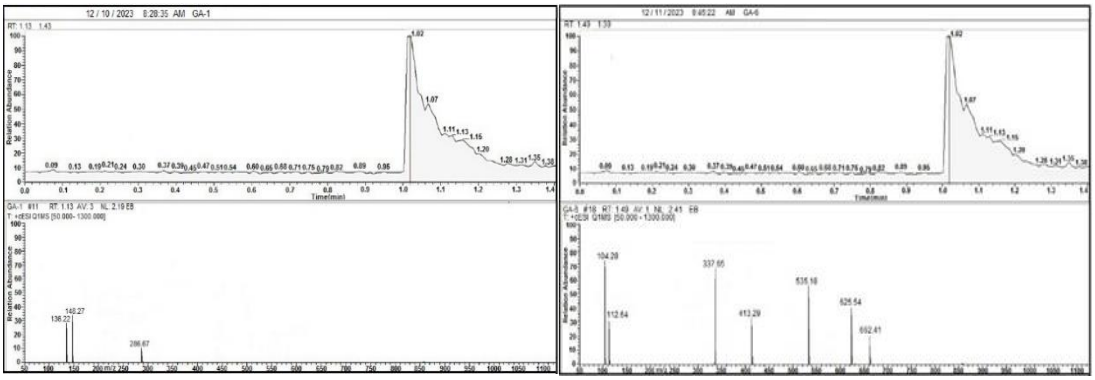

Figure 2: Mass spectrum of the ligand (HL) **Figure 3:** Mass spectrum of Fe-complex

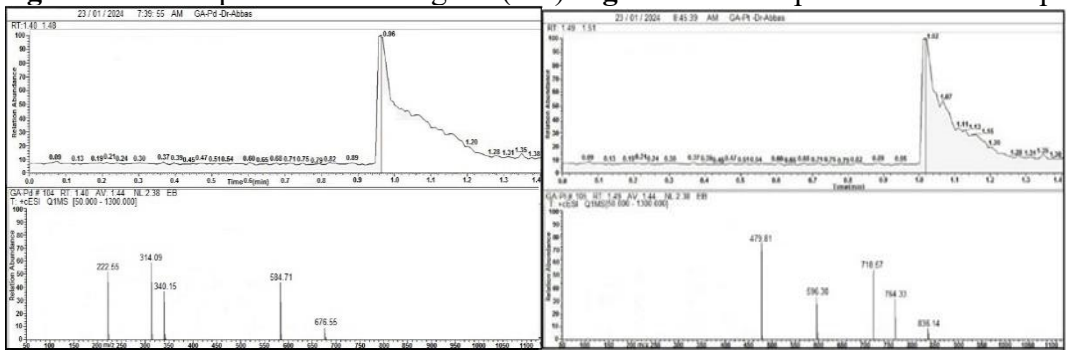

Figure 4 : Mass spectrum of Pd-complex **Figure 5** : Mass spectrum of Pt-complex

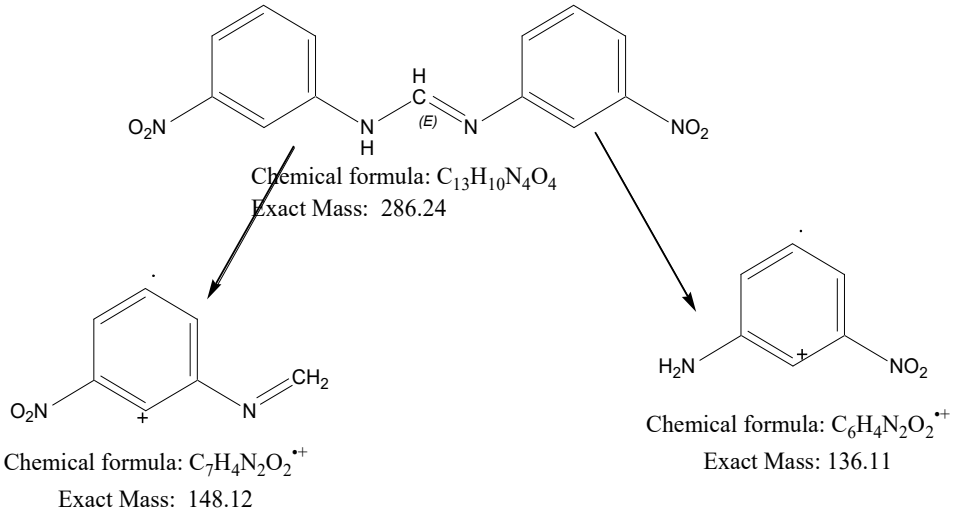

Scheme -2 Fragmentation of ligand (HL)

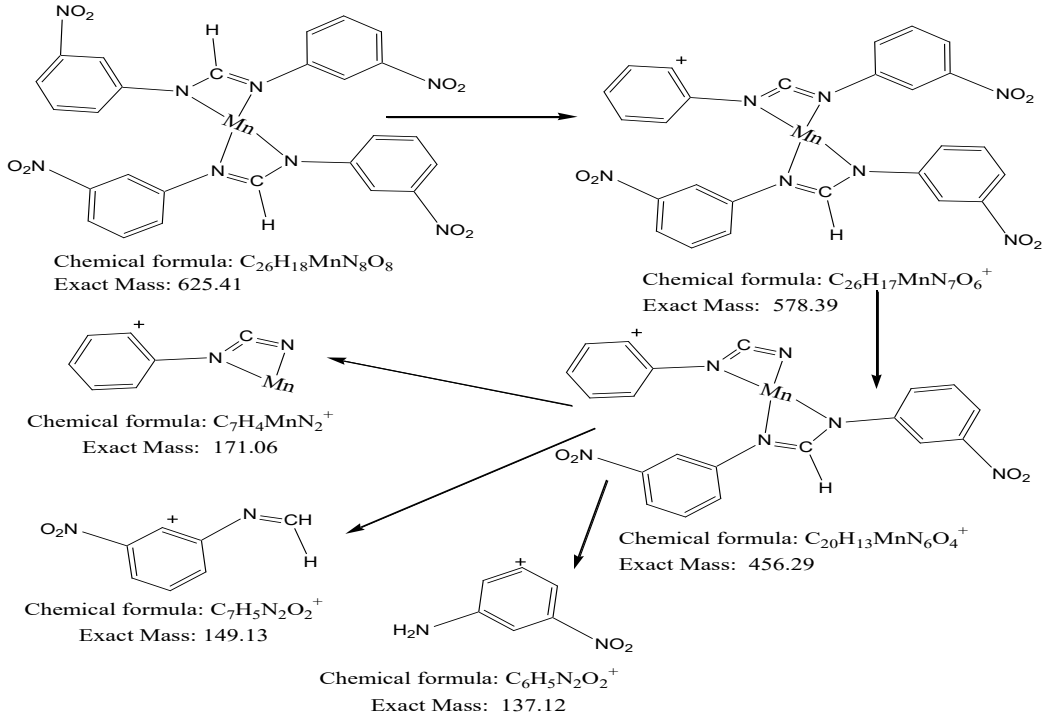

Scheme 3 : Fragmentation of Mn-complex

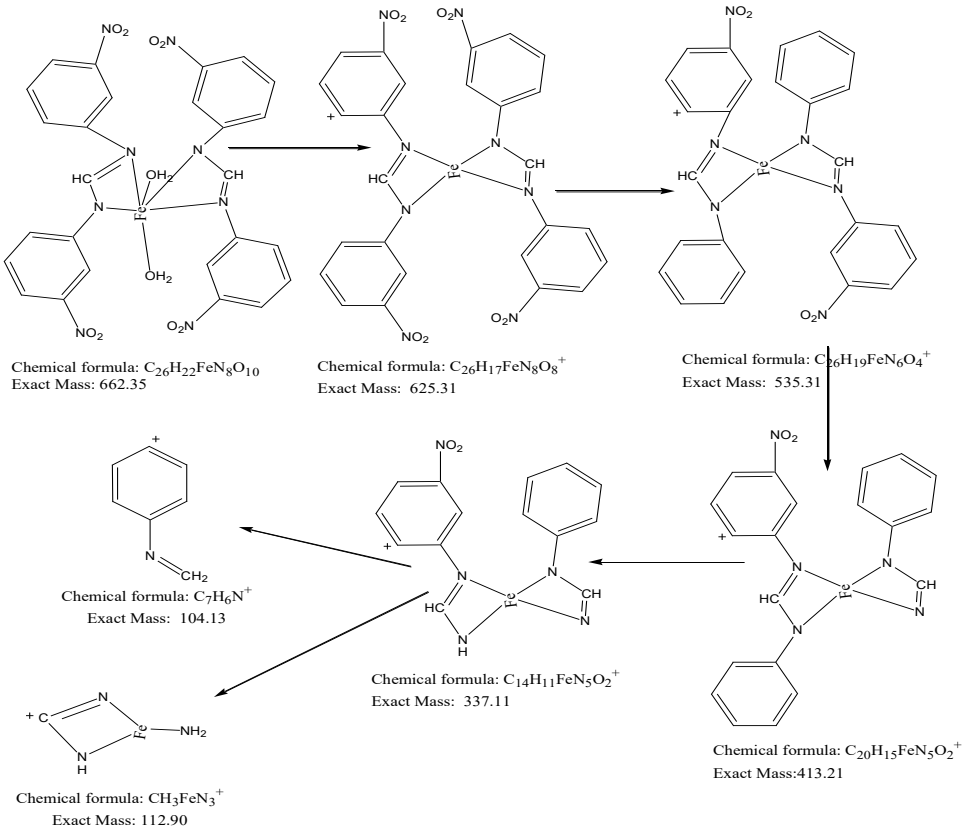

Scheme 4 : Fragmentation of Fe-complex

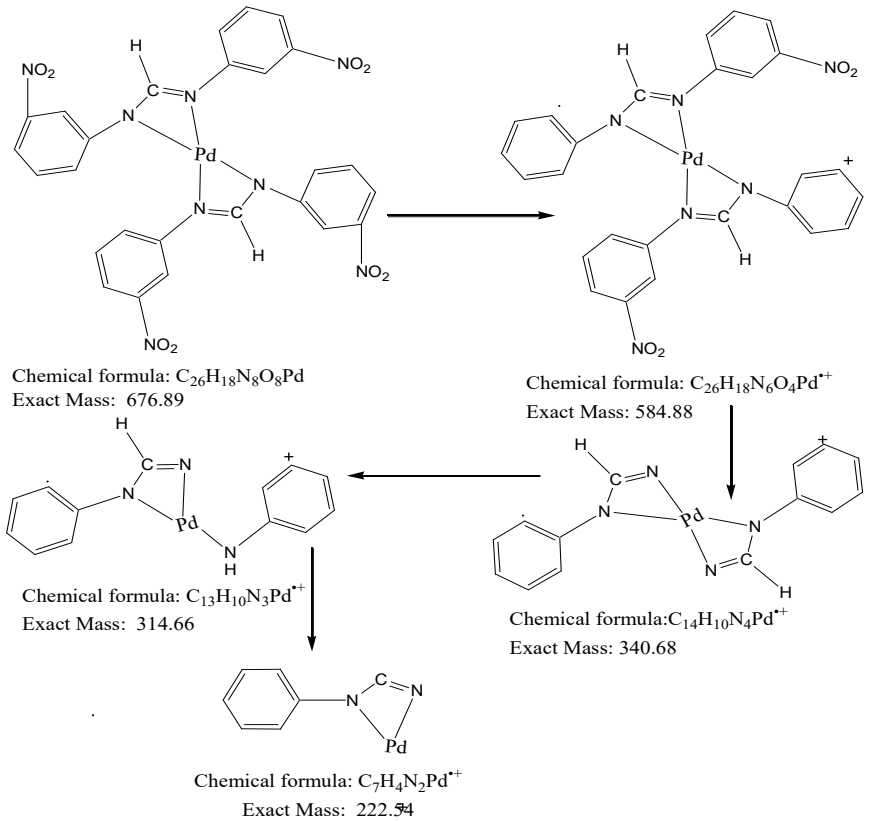

Scheme 5: Fragmentation of Pd-complex

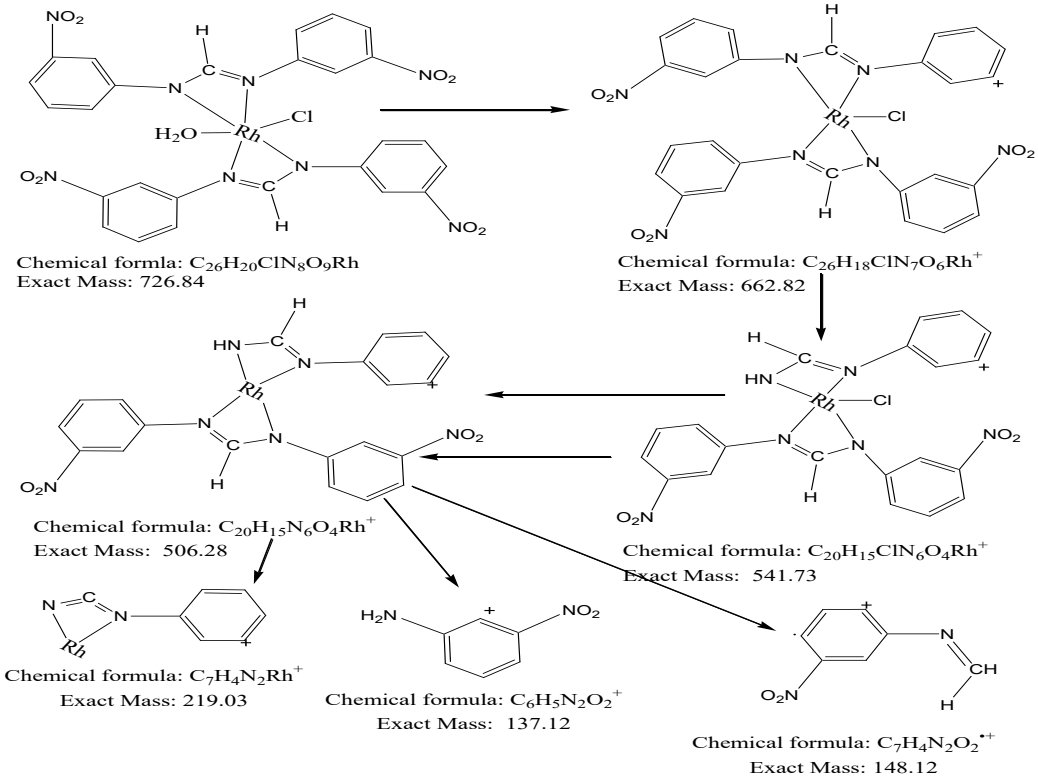

Scheme 6: Fragmentation of Rh-complex

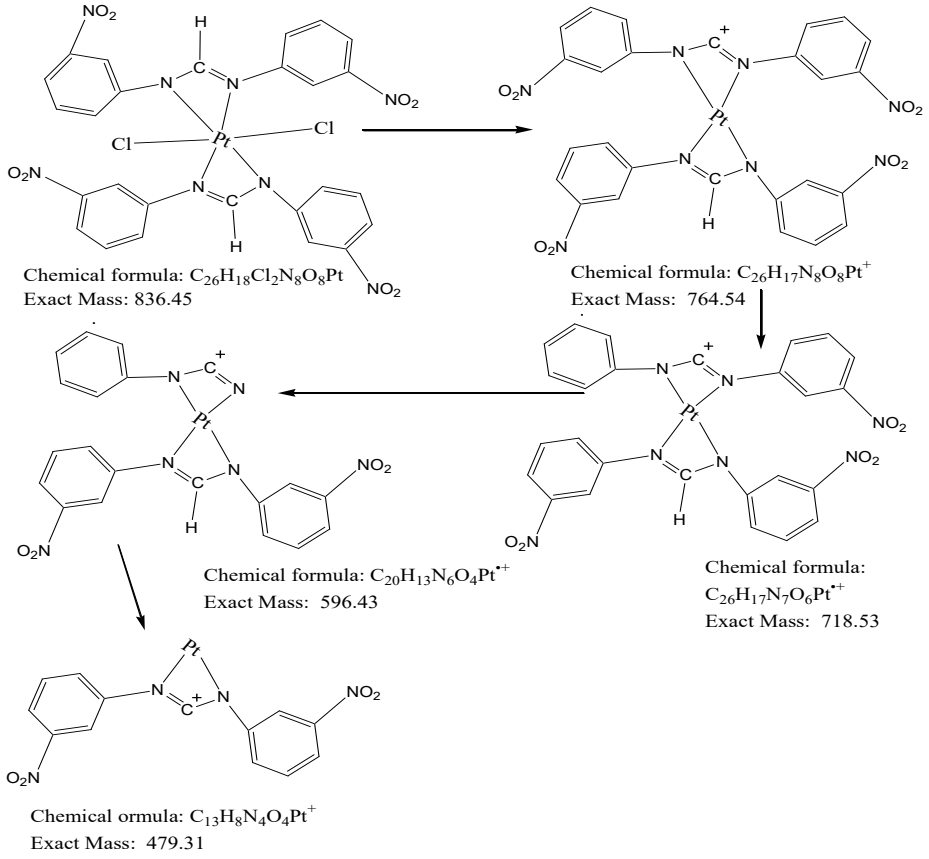

Scheme 7 : Fragmentation of Pt-complex

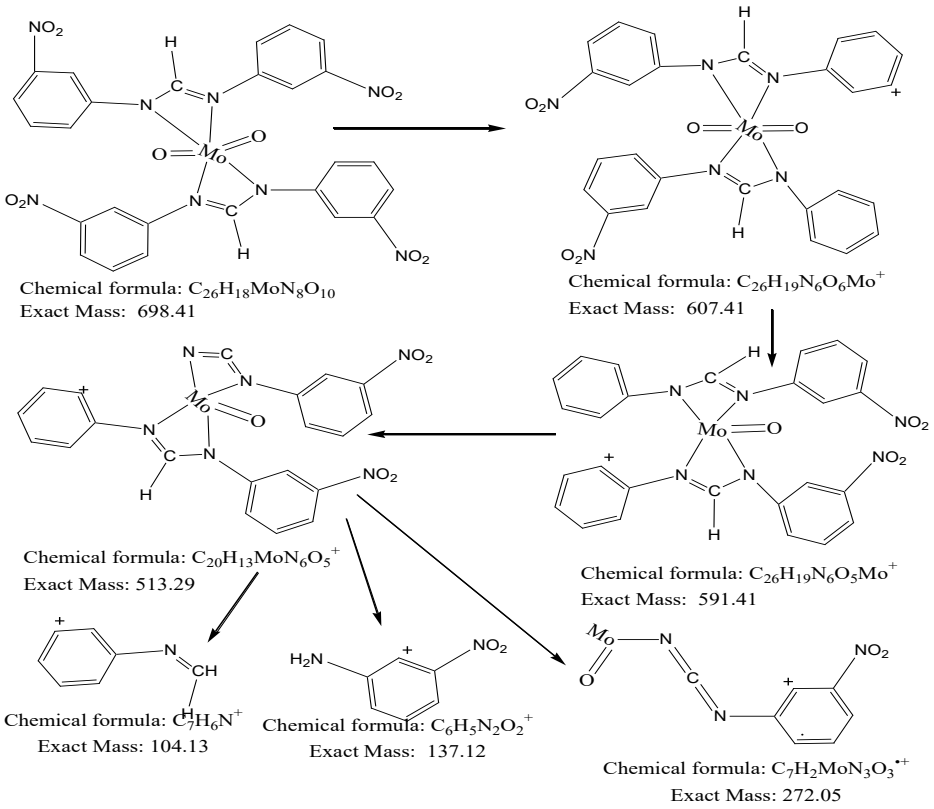

Scheme 8 : Fragmentation of Mo-complex

3.3Thermal Study Data

Thermal analysis results of the ligand (HL) and the corresponding complexes are presented in the Tables 2 and 3, as well as Figs. 6 and 7 respectively. The percentages of the weight loss for the complex, along with breakdown products, temperature ranges, and phases of decomposition were calculated up on the thermograms, and they demonstrated consistency among their predicted values and thermal decomposition consequences, validating the findings of the elemental analysis and the proposed Equations [20 and 21]. In this study, carbon was identified as the residual ligand, and Fe^+(II)was the enduring metal oxide in the ligand and metal combination. The thermogravimetric test findings show that the ligand and complexes break down in one to two steps.as showed in Scheme. 9.

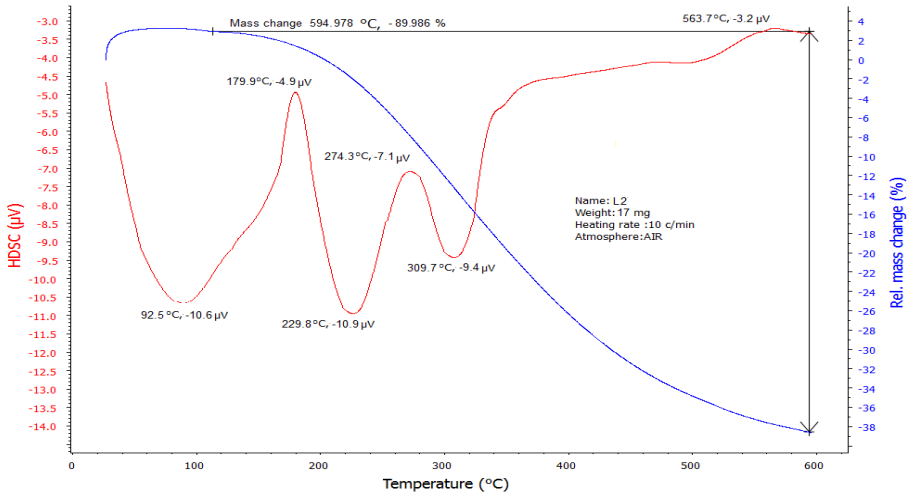

Figure 6: TGA and DSC curve of Ligand (HL)

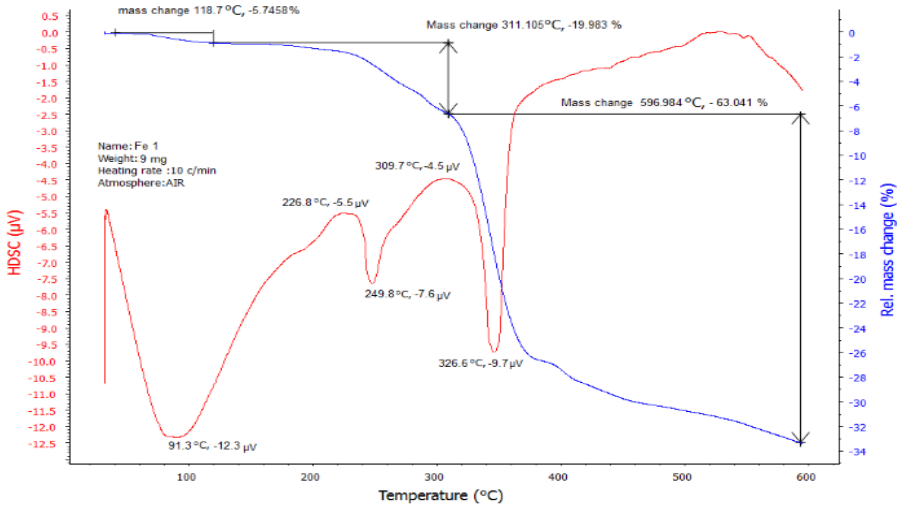

Figure 7 : TGA and DSC curve of Fe-complex

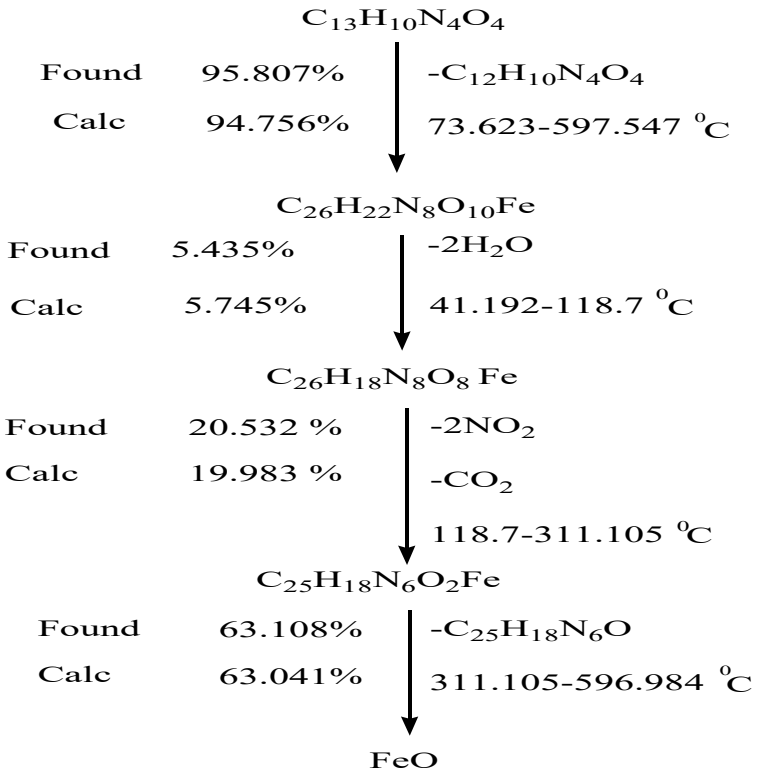

Scheme 9 : Reaction of tentative breakdown of metal and ligand complex

Table 2: TGA data of the ligand (HL) and its complex

Compounds	Step	T_i/°C	T_f/°C	Weight mass loss % Calc	found	Reaction
Ligand	1	73.623	597.547	94.756%	95.807%	$-C_{12}H_{10}N_4O_4$
C						
Calculated:94.756 % Final=5.244%; Estimated 95.807% Final =4.193%						
Fe-complex	1	41.192	118.7	5.745%	5.435%	$-2H_2O$
	2	118.7	311.105	19.983%	20.532%	$-2NO_2$, CO2
	3	311.105	596.984	63.041%	63.108%	$-C_{25}H_{18}N_6O$
FeO						
Calculated:88.769% Final=11.231%; Estimated 89.075% Final 10.925%						

Table 3: DSC data of the ligand (HL) and its complex

	T_i	T_f	T_{heat}	Type reaction
L	36.34	168.17	92.5	endothermic
	168.17	191.33	179.9	exothermic
	191.33	258.63	229.8	endothermic
	258.63	284.52	274.3	exothermic
	284.52	343.22	309.7	endothermic
Fe-complex	37.5	194.8	91.3	endothermic
	194.8	242.5	268.8	exothermic
	242.5	277.3	349.8	endothermic
	277.3	322.1	309.7	exothermic
	322.1	378.7	326.6	endothermic

3.4 Infrared Spectra Measurements:

Infrared spectral analyses were conducted on the formamidine ligand and its metal chelate complexes with Mn (II), Fe (II), Pd (II), Rh (III), Pt (IV), and Mo (VI), with the comprehensive results presented in Table 4, the ligand spectrum illustrated in Figure 8, and the Iron complex spectrum depicted in Figure 9. The ligand had band at 2939 cm^{-1} allocated for ν (N=C-H), a strong peak at 3435 cm^{-1} assigned for ν (NH), indicating the existence of the parent formamidine, 3088 cm^{-1} ν(CH) aromatic, 1681 cm^{-1} ν(C=N), 1352 cm^{-1} (C-N), 1479 cm^{-1} ν (C=C aromatic), 1523cm^{-1} ν(N=O). Infrared spectra for all the produced compounds were shown that the two sides of the formamidine ligand attached to metal ions. The nitrogen position of the formamidine group, and the trans nitrogen position deprotonating of the amine. New bands allocated to (M-N) acted at 663, 673,673,669,669,673 cm^{-1} for the Mn^{+2}, Fe^{+2}, Pd^{+2}, Rh^{+3}, Pt^{+4} ,Mo^{+6} complexes correspondingly, ν (N=O) for the free ligand was located at 1523cm^{-1} while for the complexes the ν (N=O) found at 1523 cm^{-1}, 1529 cm^{-1}, 1531 cm^{-1}, 1523 cm^{-1}, 1523 cm^{-1},1525 cm^{-1} respectively. Other bands were 320cm^{-1} ν (Rh-Cl), and 318cm^{-1} ν (Pt-Cl) [22 and 23].

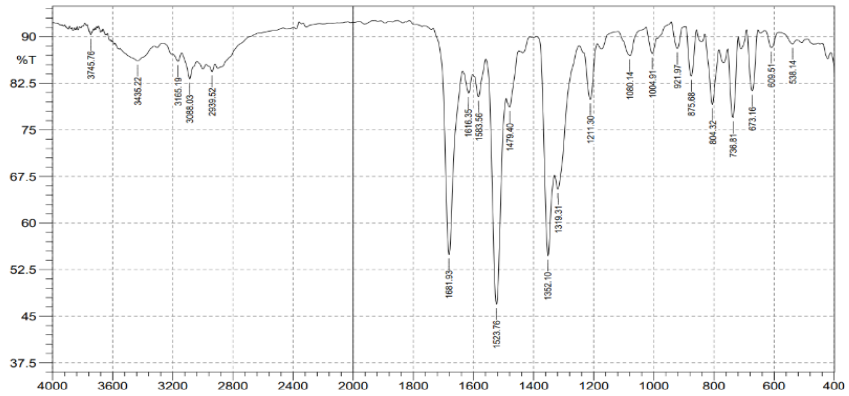

Figure 8: FT-IR spectrum of ligand (HL)

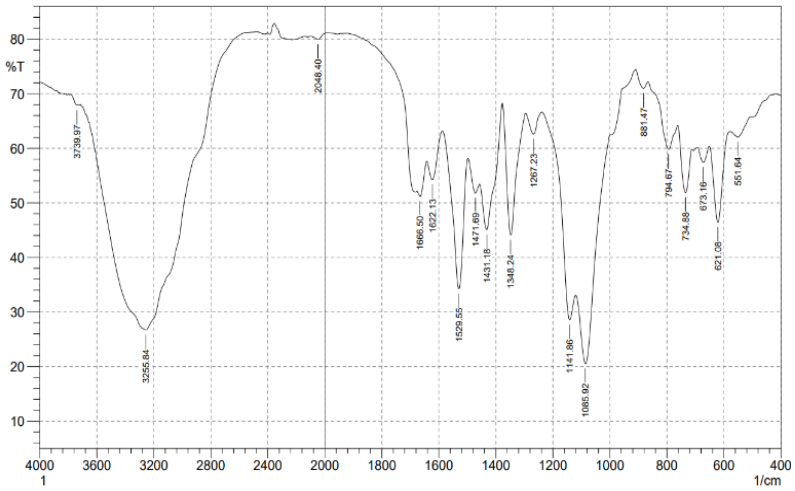

Figure 9: FT-IR spectrum of complex (Fe)

Table 4: The IR spectra bands (cm^{-1}) of the Formamidine ligand and its complexes

Compounds	ν (H_2O) aqua	ν (N=C-H)	ν (NH)	ν (CH) aromatic	ν (C=N)	ν (C-N)	ν (C=C)	ν (N=O)	Other bands
HL	------	2939	3435	3088	1681	1352	1479	1523	--------
[Mn(L)$_2$]		2900	-----	3095	1675	1344	1483	1523	663(Mn-N)
[Fe(L)$_2$(H_2O)$_2$]	3255 1622 805	2927	-----	3097	1666	1348	1473	1529	673 (Fe-N)
[Pd(L)$_2$]		2779	-----	3051	1671	1350	1475	1531	673 (Pd-N)
[Rh(L)$_2$(H_2O)(Cl)]	3218 1623 813	2929	-----	3074	1668	1350	1483	1523	669 (Rh-N) 320(Rh-Cl)
[Pt(L)$_2$(Cl)$_2$]		2974	-----	3099	1691	1348	1485	1523	669(Pt-N) 318(Pt-Cl)
[Mo(L)$_2$(O)$_4$]		2941		3087	1681	1350	1475	1525	673(Mo-N)

3.5 UV-Vis Studies of the Ligand (HL) and its Complexes:

The electronic spectrum for ligand (HL) in Fig.10 reveals robust absorptions at 293 nm, 34129.692 cm^{-1} ascribed to the n→ π*. The electronic alteration of Mn^{+2} complex is revealed a peak of 263, 381, 625, 863,887, 993 nm assigned to n→ π*, C.T M→L ,$^6A_1g \rightarrow {}^4Eg_{(G)}$, $^6A_1g \rightarrow {}^4T_2g_{(G)}$ $^6A_1g \rightarrow {}^4T_1g_{(G)}$ $^6A_1g \rightarrow {}^4T_2g_{(D)}$, respectively, which is an indicative of a

tetrahedral geometry [24]. The Fe^{+2} complex in Fig.11 showed peaks of 475, 720, 800 nm assigned to $^6A_1g \rightarrow {}^4T_2g_{(G)}$, $^6A_1g \rightarrow {}^4T_1g_{(G)}$, $^6A_1g \rightarrow {}^4Eg_{(D)}$ respectively. It is also representing an octahedral geometry [25]. The Pd^{+2} complex presented appeared peaks of 263, 391, 977, 999 nm assigned to π→π*, n→π* C.T M→L,$^1A_1g \rightarrow {}^1B_1g$,$^1A_1g \rightarrow {}^1A_2g$ respectively, which represents a Square planar geometry. The Rh^{+3} complex showed peaks of 263, 396, 542, 629, 726 nm assigned to π→π*, n→ π*, L-M (C.T), $^1A_1g \rightarrow {}^1T_1g$,$^1A_1g \rightarrow {}^1T_2g$, $^1A_1g \rightarrow {}^1T_3g$ respectively, it depicts an octahedral geometry. The Pt^{+4} complex showed peaks of 265, 415, 889,993 nm assigned to n→ π*, $^1A_1g \rightarrow {}^1T_1g$, $^1A_1g \rightarrow {}^1T_2g$, $^1A_1g \rightarrow {}^1T_3g$ respectively, it depicts an octahedral geometry. The Mo^{+6} complex showed peaks of 212, 288, 542 nm assigned to π→π*, n→π*, C. T M→L respectively, it depicts an octahedral geometry [26]. Table 5. shows the electronic assignment for metal complexes.

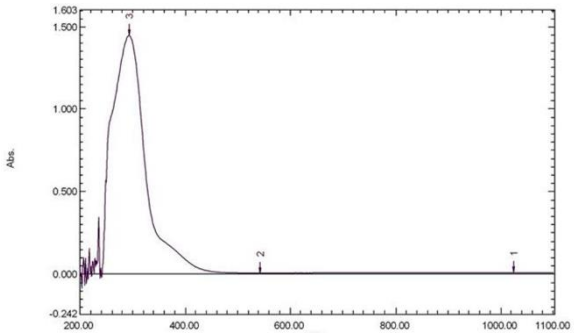

Figure 10 : UV-Vis spectrum of ligand (HL)

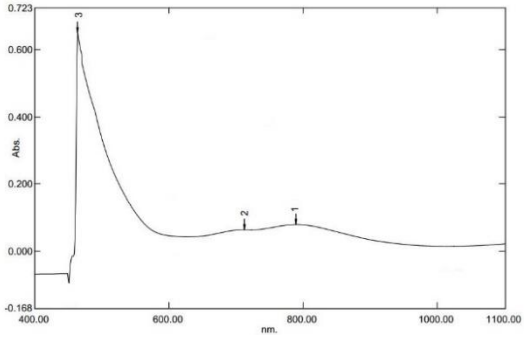

Figure 11 : UV-Vis spectrum of Fe-complex

Table 5: UV-Vis spectra, magnetic moments and molar conductivity for ligand (HL) and their metal complexes

Compound	λ nm	ύ cm^{-1}	Abs	Ɛmax L mol^{-1} cm^{-1}	Assignment	*μeff* (B.M)
Ligand = HL	293	34129.692	1.449	144.9	n→ π*	
$[Mn(L)_2]$ Tetrahedral	263 381 625 863 887 993	38022.813 26246.719 16000 11587.485 11273.957 10070.493	3.285 0.472 0.033 0.008 0.010 0.057	328.5 47.2 3.3 0.8 1 5.7	n→π* C.T M→L $^6A_1g \rightarrow {}^4Eg_{(G)}$ $^6A_1g \rightarrow {}^4T_2g_{(G)}$ $^6A_1g \rightarrow {}^4T_1g_{(G)}$ $^6A_1g \rightarrow {}^4T_2g_{(D)}$	5.792
$[Fe\ (L)_2\ (H_2O)_2]$ Octahedral	475 720 800	21052.631 13888.888 12500	0.66 0.05 0.07	66 5 7	C.T M→L ($^5T_2g \rightarrow {}^5Eg$)	5.568
$[Pd\ (L)_2]$ Square planar	263 391 977 999	38022.813 25575.447 10235.414 10010.01	2.201 0.318 0.034 0.033	220.1 31.8 3.4 3.3	π→π* n→π* C.T M→L $^1A_1g \rightarrow {}^1B_1g$ $^1A_1g \rightarrow {}^1A_2g$	Dia
$[Rh\ (L)_2\ (H_2O)\ (Cl)]$ Octahedral	263 396 542 629 726	38022.813 25252.525 18450.184 15898.251 13774.104	1.315 0.253 0.020 0.020 0.025	131.5 25.3 2 2 2.5	π→π* n→π*+C. T M→L $^1A_1g \rightarrow {}^1T_1g$ $^1A_1g \rightarrow {}^1T_2g$ $^1A_1g \rightarrow {}^1T_3g$	Dia
$[Pt(L)_2\ (Cl)_2]$ Octahedral	265 415 889 993	37735.849 24096.385 11248.593 10070.493	0.484 0.344 0.007 0.017	48.4 34.4 0.7 1.7	n→π* $^1A_1g \rightarrow {}^1T_1g$ $^1A_1g \rightarrow {}^1T_2g$ $^1A_1g \rightarrow {}^1T_3g$	Dia
$[Mo(L)_2\ (O)_4]$ Octahedral	212 288 542	47169.811 34722.222 18450.184	0.641 1.103 0.002	64.1 110.3 0.2	π→π* n→π* C. T M→L	Dia

3.6 Study of antioxidant activity using DPPH method

The antioxidant activity of the ligand and its metal complexes was evaluated using Gallic acid as a reference standard, given its phenolic nature. Five standard solutions with varying amounts of Gallic acid (0.008, 0.004, 0.002, 0.001 and 0.0005 $mmol^{-1}$) were produced using ethanol as a diluent from a 10 $mmol^{-1}$ solution of Gallic acid. 100 µL of each of the standard Gallic acid solutions were mixed with 6 ml of 45 µg ml^{-1} DPPH solution. After the combined solution was let to sit at room temperature for thirty minutes in the dark, the reaction mixture's absorbance was measured at 517 nm. Figs. 12 and 13. demonstrating that a lower IC_{50} value indicates DPPH radical scavenging, which means the Fe complex is more antioxidant active [27 and 28]. The results are as follows (Gallic acid >HL>Fe complex >Mo complex >Mn complex >Rh complex >Pd complex >Pt complex), The lower the IC_{50} value, the more inhibiting the ratios are which detailed in Table 6 and Figure-14 Mechanical ligand.

Table 6: Antioxidant activity of formamidine and its complexes

compound	Concentration	PI%	RSA%	IC_{50} values mg/mL
Gallic acid	0.008	11.58	88.42	0.008
	0.004	44.82	55.18	
	0.002	63.19	36.81	
	0.001	70.58	29.42	
	0.0005	76.06	23.94	
L	0.061	21.05	78.95	0.026
	0.030	38.43	61.57	
	0.015	45.48	54.52	
	0.008	53.12	46.88	
Mn-Complex	0.008	22.49	77.51	0.094
	0.004	30.28	69.72	
	0.002	51.25	48.75	
	0.001	60.29	39.71	
Fe-Complex	0.064	20.46	79.54	0.039
	0.032	40.43	59.57	
	0.016	46.03	53.97	
	0.008	54.18	45.82	
Pd-Complex	0.012	19.13	80.87	0.227
	0.006	32.19	67.81	
	0.003	60.28	39.72	
	0.0015	61.06	38.94	
Rh-Complex	0.008	21.09	78.91	0.182
	0.004	33.19	66.81	
	0.002	55.18	44.82	
	0.001	72.82	27.18	
Pt-Complex	0.012	18.49	81.51	0.727
	0.006	33.19	66.81	
	0.003	57.13	42.87	
	0.0015	60.29	39.71	
Mo-Complex	0.008	22.49	77.51	0.077
	0.004	33.19	66.81	
	0.002	55.15	44.85	
	0.001	60.29	39.71	

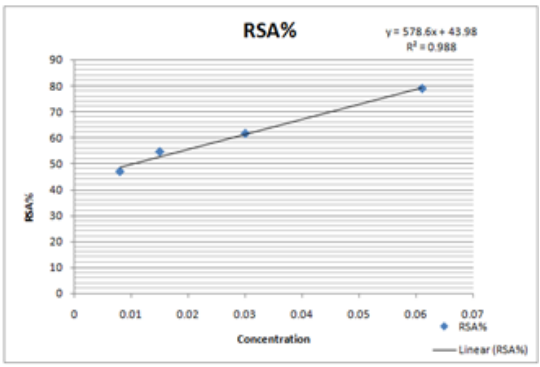

Figure 12 : Antioxidant activity of (HL)

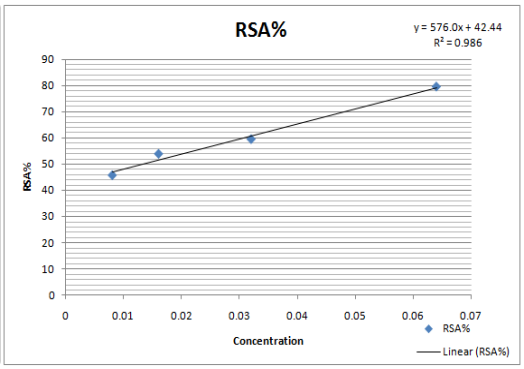

Figure 13 : Antioxidant activity of Fe^{+2} Complex

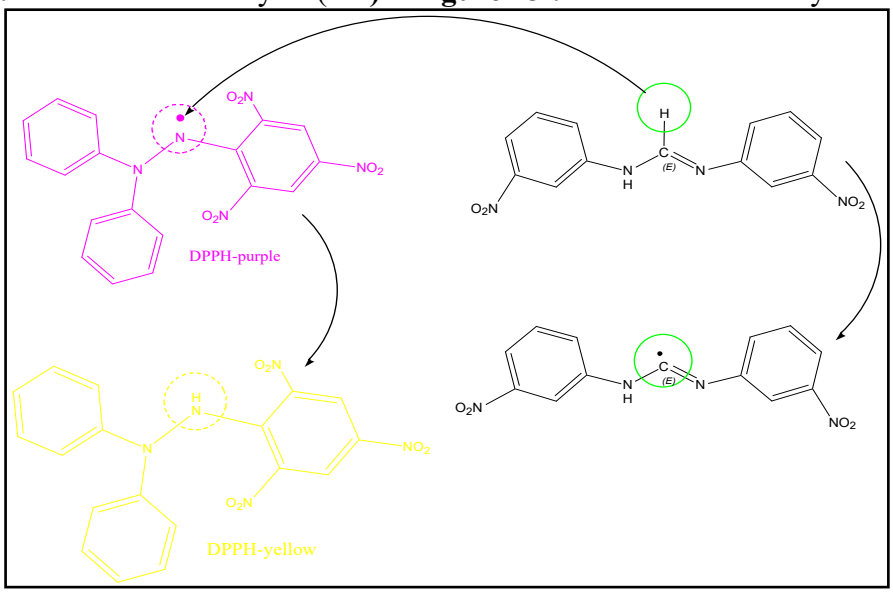

Figure14 : Mechanical ligand

3.7Antimicrobial activity of the ligand and its complexes

The biological activity of the formamidine and its complexes was investigated against *Escherichia coli* as Gramme negative bacteria and *Staphylococcus aureus* as Gramme positive bacteria. In addition to the fungi examination on *Aspergillus Niger*. Antibacterial activity of formamidine was similarly demonstrated the inhibition zone values against *Escherichia coli* and *Staphylococcus aureus*; however, when the complexes were compared with the free ligand, activity was in complexes and no effect appeared on the ligand, as shown in the Fig. 15. According to Tweedy's chelation theory, the enhanced activity of the complexes can be attributed to the formation of metal-ligand coordination bonds [29 and 30]. The complexes and ligands both showed activity against the fungi as shown in Fig. 16 and detailed in Table 7.

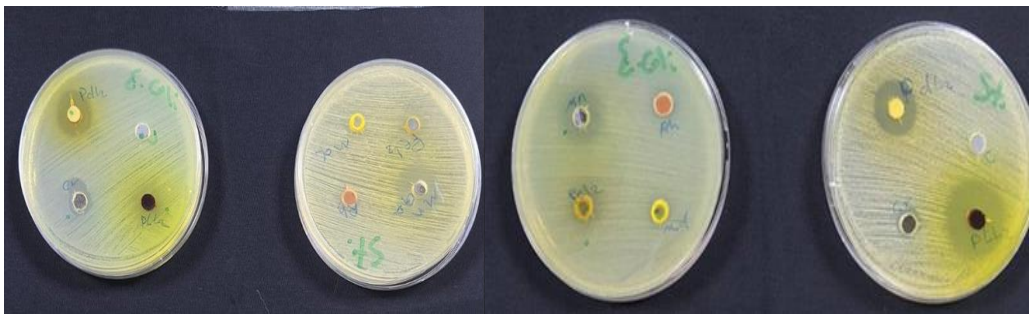

Figure 15 : Effect of the ligand and its complexes towards

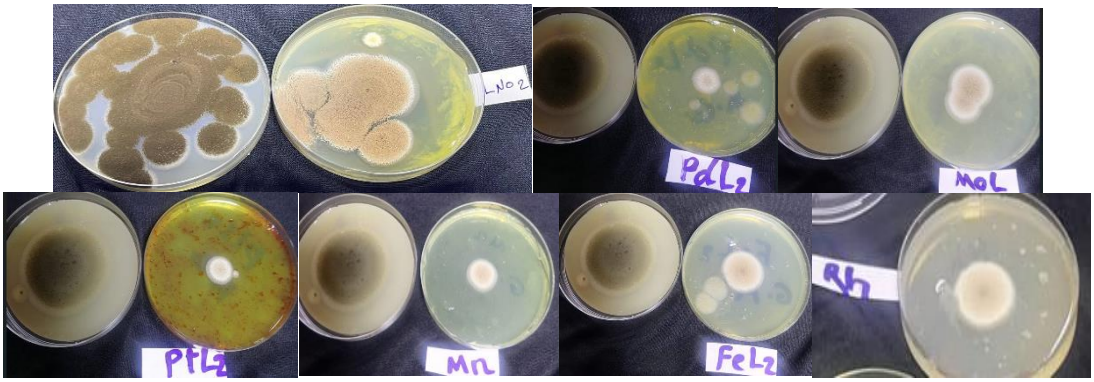

Figure 16: Effect of the ligand and its complexes towards fungi

Table 7: Antibacterial activity and anti-fungi data of ligand and its complexes (inhibition zone)

Compound	*Staphylococcus* aureus G+	*Escherichia* Coli G−	Fungi
L	No	No	50mm
[Mn $(L)_2$]	1.5x1.3	1.4x1.4	20mm
[Fe $(L)_2$ $(H_2O)_2$]	No	No	25mm
[Pd $(L)_2$]	1.7x1.8	1.7x1.8	15mm
[Rh $(L)_2$ (H_2O) (Cl)]	No	No	30mm
[Pt $(L)_2$ $(Cl)_2$]	2.3x2.5	No	13mm
[Mo$(L)_2(O)_4$]	No	No	27mm

Conclusion

In conclusion, the formamidine ligand was easily synthesized through the reaction of triethyl orthoformate and *m*-nitroaniline. This ligand subsequently coordinated with various metal ions (Mn^{+2}, Fe^{+2}, Pd^{+2}, Rh^{+3}, Pt^{+4} and Mo^{+6}) forming air-stable compounds with distinct morphologies. Ligand and metal complexes were identified using a range of analytical techniques, including elemental microanalysis, magnetic susceptibility, thermal analysis TGA and DSC curves, FTIR, UV-Vis, ^{1}H-NMR, and metal-chloride containing electrical conductivity and melting point measurement. The M: L percentage in all compounds existed 1:2. Agreeing with the results, the geometric shape is proposed to be octahedral for (Fe^{+2}, $Rh^{+3,}$ Pt^{+4}, Mo^{+6}) square planer for (Pd^{+2}) and tetrahedral for (Mn^{+2}) that was based on the data from mass and IR measurements. The biological activity of the corresponding complexes against fungi and bacteria was performed, as well as antioxidants study has carried out using Gallic acid. Fungi gave more inhibition than bacteria. The synthesized complexes can be considered as potentially candidates to be used in the future in medical and catalytic applications.

References:

[1] A.S.Mali , P.Bandivadekar , G.U.Chaturbhuj, "Aluminized Polyborate: A New and Eco-friendly Catalyst for the Synthesis of Symmetrical N, N'-Di (aryl/alkyl) formamidines", *Organic Preparations and Procedures International*, vol. 54, no.3, pp. 242-248,2022.

[2] W. Guo, "Base mediated direct C–H amination for pyrimidines synthesis from amidines and cinnamaldehydes using oxygen as green oxidants", *Chinese Chemical Letters*,vol.27, no.1, pp.47-50, 2016.

[3] J.A.Aboyewa, N.R.Sibuyi, M.Meyer, O.O.Oguntibeju, "Green synthesis of metallic nanoparticles using some selected medicinal plants from southern africa and their biological applications", *Plants*, vol.10, no.9, pp.1929,2021.

[4] M.L. Cole, A.I. McKay, N.S. Ping, "Coordinative versatility in main group complexes of C-2, 6-terphenyl substituted amidinates Polyhedron'', vol.170, pp. 424-430, 2019.

[5] S.D .Oladipo, S.J .Zamia , A.A. Badeji, M.A .Ejalonibu, A.A .Adeleke, I.A .Lawal, et al., "Ni^{2+} and Cu^{2+} complexes of N-(2, 6-dichlorophenyl)-N-mesityl formamidine dithiocarbamate structural and functional properties as CYP3A4 potential substrates'', *Scientific Reports*,vol.13, no.1, pp.13414, 2023.

[6] F.T. Edelmann, " Lanthanides and actinides: Annual survey of their organometallic chemistry covering the year 2014'', *Coordination Chemistry Reviews*, vol. 306, pp. 346-419,2016.

[7] A.Mequanent, "General veterinary pharmacology and drugs used for treatment of bacteria, virus, fungus and parasites in animals", *Life Sci J*, vol.19, pp.45,2022.

[8] Q. Li, Z. Li, " Molecular packing: another key point for the performance of organic and polymeric optoelectronic materials'', *Accounts of chemical research*, vol.53, no.8, pp. 962-973, 2020.

[9] S. Dong, X. Feng, X. Liu, " Chiral guanidines and their derivatives in asymmetric synthesis'', *Chemical Society Reviews*, vol. 47, no.23, pp.8525-8540, 2018.

[10] S. Rajak, K. Chair, L.K. Rana, P. Kaur, T. Maris, A. Duong, " Amidine/Amidinate Cobalt Complexes: One-Pot Synthesis, Mechanism, and Photocatalytic Application for Hydrogen Production'', *American Chemical Society*, vol.59, no.20, pp.14910-14919, 2020.

[11] H.Li, H.Guo, Z.Fang, T.M.Aida, R.L.Smith, "Cycloamination strategies for renewable N-heterocycles'', *Royal Society of Chemistry*, vol.22, no.3, pp.582-611, 2020.

[12] U.Yolsal, , T.A .Horton, M. Wang, M.P. Shaver, "Polymer-supported Lewis acids and bases: Synthesis and applications'' *Progress in Polymer Science*, vol.111, pp. 101313, 2020.

[13] A.A .Jawad, A.J Alabdali, "Synthesis, Characterization and Antibacterial Activity of Some Penicillin Derivatives'', *Al-Nahrain Journal of Science,* vol.23, no.4, pp.29-34, 2020.

[14] N.M. Mallikarjuna , J. Keshavayya, " Synthesis, spectroscopic characterization and pharmacological studies on novel sulfamethaxazole based azo dye" , *Journal of King Saud University- Science*, vol. 32, pp. 251-259, 2020.

[15] I.S. Hamza, W.A. Mahmmoud, A.A.S. Al-Hamdani, S.D. Ahmed, A.W Allaf, W. Al Zoubi, "Synthesis, characterization, and bioactivity of several metal complexes of (4-Amino-N-(5-methyl-isaxazol-3-yl)-benzenesulfonamide) '', *Inorganic Chemistry Communications,* vol. 144, pp.109776, 2022.

[16] S.M. Mahdi , A.K. Ismail, "Preparation and Identification of new azo-schiff base ligand (NASAR) and its divalent transition metal Complexes '', *Journal of Pharmaceutical Sciences and Research*, vol. 10, no. 9, pp. 2175-2178, 2018.

[17] B.Wang, P.Z .Zhang, J.M. Xia, A.Q. Jia, Q.F. Zhang, "Synthesis, photochemical characterization, and thermal stability of a series of substituted formamidines as ultraviolet light absorbers'', *Journal of Vinyl and Additive Technology*, vol.25 ,no.2 , PP.108-113, 2019.

[18] S.M. Obaid, A.J. Jarad, A.A.S. Al-Hamdani, "Synthesis, characterization and biological activity of mixed ligand metal salts complexes with various ligands'', *In Journal of Physics: Conference Series* ,Vol. 1660, no. 1, p. 012028, 2020.

[19] O.A.EL-Gammal, H.Alshater, H.A. El-Boraey, "Schiff base metal complexes of 4-methyl-1H-indol-3-carbaldehyde derivative as a series of potential antioxidants and antimicrobial: Synthesis, spectroscopic characterization and 3D molecular modeling'', *Journal of Molecular Structure*, vol.1195, 220-230, 2019.

[20] C.Lv , L.Zhong ,H. Liu ,Z. Fang , C.Yan , M. Chen , et al, "Selective electrocatalytic synthesis of urea with nitrate and carbon dioxide'', *Nature Sustainability*, vol.4, no.10, pp.868-76,2021.

[21] M. R. Gyton, A. R. Leverett, M. L. Cole, and A. I. McKay, "Bulky bis (aryl) triazenides: just aspiring amidinates? A structural and spectroscopic study'', *Dalton Transactions*, vol.49, no.17, pp.5653-5661, 2020.

[22] R.K.H. Al-Daffaay, "Preparation, spectroscopic characterization of transition metal complexes with Schiff base 2-[1-(1H-indol-3-yl)ethylimino)methyl]naphthalene-1-ol'', *Baghdad Science Journal*, vol. 20 no. 7, pp. 1036-1044, 2022

[23] B. Wang, P.Z. Zhang, J.M. Xia, A.Q. Jia, Q.F. Zhang, "Synthesis, photochemical characterization, and thermal stability of a series of substituted formamidines as ultraviolet light absorbers", *Journal of Vinyl and Additive Technology*, vol.25, no.2, pp.108-113, 2019.

[24] B. R. Bade, S. R. Rondiya, K. B. Kore, D. S. Nilegave, M. P. Nasane, S. B. Jathar, A. M. Funde, "Room temperature synthesis of formamidinium lead iodide (FAPbI3) perovskite for low-cost absorber in solar cells",*ES Energy Environment*, vol.13, pp.31-36, 2021.

[25] M. R Maliyappa, J, Keshavayya, N. M., Mallikarjuna, P. M Krishna, N., Shivakumara, T . Sandeep,et al, "Synthesis, characterization, pharmacological and computational studies of 4, 5, 6, 7-tetrahydro-1, 3-benzothiazole incorporated azo dyes", *Journal of Molecular Structure*,vol.1179, pp.630-64 ,2019.

[26] S. K. Kyei, O .Akaranta, G. Darko, "Synthesis, characterization and antimicrobial activity of peanut skin extract-azo-compounds",*Scientific African*, vol.8, pp.00406, 2020.

[27] A. G. Prashantha, J. Keshavavayya and R. A. S. Ali, "Synthesis, spectral characterization and biological applications of novel 3-[(4,6-dihdroxy pyrimidin-5-yl) diazenyl]-4-methylbenzoic acid azo dye and their derivatives" , *Results in chemistry*, vol. 3, no. 100110, pp.1-11, 2021.

[28] S. D .Oladipo, B .Omondi, C. Mocktar, "Synthesis and structural studies of nickel (II)-and copper (II)-N, N′-diaryl formamidine di thiocarbamate complexes as antimicrobial and antioxidant agents", *Polyhedron*, vol.170, pp.712-722, 2019.

[29] U. Bongoza, S. J. Zamisa, W. A. Munzeiwa, B.Omondi, "Silver (I) complexes of N, N′-diarylformamidine ligands: Synthesis, crystal structures, and in vitro antibacterial studies", *Applied Organometallic Chemistry*, vol.36 no. 7, pp.6726, 2022.

[30] S. D. Oladipo, B. Omondi, C. Mocktar, "Co (III) N, N′-diarylformamidine dithiocarbamate complexes: Synthesis, characterization, crystal structures and biological studies", *Applied Organometallic Chemistry*, vol.34 no.(5), pp.5610, 2020